Sensors and Materials, Vol. 36, No. 1 (2024) 251–260
MYU Tokyo

S & M 3515

Energy Spectroscopy for Low-energy Photons Using Diamond Detector Combined with Micro-CMOS Preamplifier

Kengo Oda,[1*] Junichi H. Kaneko,[1] Daisuke Matsunaga,[2]
Takanori Hanada,[1] Tsukasa Mizukoshi,[1] and Shintaro Hirano[1]

[1]Graduate School of Engineering, Hokkaido University,
Kita 13 Nishi 8, Kita-ku, Sapporo, Hokkaido 060-8628, Japan
[2]Horiba, Ltd., 2, Kisshoin Miyano-Higashimachi, Minami-ku, Kyoto, Kyoto 601-8510, Japan

(Received October 4, 2023; accepted January 5, 2024)

Keywords: diamond, radiation detector, low-energy photons, soft X-ray, CMOS preamplifier

To measure soft X-ray energy spectra at room temperature using diamond, we connected a 300-μm-thick single-crystal CVD diamond radiation detector with excellent charge carrier transport properties to a micro–preamplifier fabricated using CMOS technology via Φ97 μm electrodes. We attempted to measure the photon energy spectrum from a few keV to 60 keV at room temperature by reducing the leakage current and the total input capacitance to the preamplifier. The energy resolution for 5.9 keV X-rays from ^{55}Fe was ΔE = (484 ± 10) eV (FWHM).

1. Introduction

Diamond has excellent features such as high radiation resistance,[1–4] high-temperature operation,[5–8] fast response,[9] and near bioequivalence,[10] and its use in accelerators, nuclear fusion, nuclear reactors, and medicine is expanding. Since single-crystal diamond fabricated by chemical vapor synthesis with excellent charge carrier transport properties has become commercially available, it has been practically used in a variety of radiation measurements, including those of alpha particles,[11,12] neutrons,[13,14] and heavy charged particles.[15,16]

One of the radiation measurement applications that uses diamond's superior characteristics is the measurement of soft X-ray energy spectra. The average electron–hole pairing energies of diamond and Si are 13.1 and 3.62 eV,[17] respectively, which means that diamond can produce only about one-third of the electron–hole pairs as silicon. On the other hand, the leakage current of diamond at room temperature is about 1/1000 of that of silicon, which means that high energy resolution can be achieved for soft X-rays at room temperature by combining diamond and an electronic circuit system with an excellent signal-to-noise ratio.

Silicon drift detectors[18] and superconducting detectors[19] have been widely studied in soft X-ray energy spectrum measurements, and very good energy resolution has been reported for both. On the other hand, the detection efficiency of superconducting detectors can be improved,

*Corresponding author: e-mail: odahokudaikengo64@eis.hokudai.ac.jp
https://doi.org/10.18494/SAM4686

ISSN 0914-4935
https://myukk.org/

and they must be operated below liquid nitrogen temperature. Silicon drift detectors have an excellent balance between energy resolution and detection efficiency, but, as mentioned above, they must usually be cooled by Peltier devices to suppress the leakage current of the silicon. If diamond can achieve the same performance as a silicon drift detector without the need for a cooling mechanism, it can be applied to X-ray fluorescence analyzers for microscopes that measure soft X-ray energy spectra in confined spaces.

There have been reports of soft X-ray measurements with radiation detectors using polycrystalline diamond,[20] which has poor charge carrier transport properties, and diamond synthesized by the hot filament CVD method.[21] Similar measurements using SiC radiation detectors have also been reported,[22] but these detectors collect charge using comb-type electrodes installed near the surface, and the effective sensitizing thickness is limited to a few microns near the surface. On the other hand, the energy range of photons in soft X-ray analysis is from keV to 10 keV order and the average free path of a 5.9 keV photon to diamond is about 300 μm. This means that it is essential to use single-crystal CVD diamond with excellent charge carrier transport properties and to use the entire crystal as a sensitized layer for practical application.

In this study, as an experiment on soft X-ray measurement using a diamond detector, we connected a 300-μm-thick single-crystal CVD diamond radiation detector with excellent charge carrier transport properties to a micro–preamplifier fabricated by CMOS technology via a Φ97 μm readout electrode. Noise was suppressed by reducing the leakage current and the total input capacitance, and an initial photon energy spectrum measurement from a few keV to 60 keV was attempted.

2. Materials and Methods

2.1 Detector concept

If the amplification factor of a preamplifier is sufficiently large, the circuit noise [equivalent noise charge (ENC)] of the preamplifier satisfies[23]

$$ENC^2 = A_1 C_t^2 \frac{2\alpha kT}{g_m}\frac{1}{\tau_S} d + A_2 C_t^2 \pi A_f + A_3 q I_{leak} \tau_S, \quad (1)$$

where A_1, A_2, and A_3 are constants determined by the shaper, C_t is the input capacitance of the preamplifier, α is a constant determined by the first-stage field effect transistor (FET), k is the Boltzmann constant, T is the temperature of the first-stage FET, g_m is the mutual conductance (gain) of the first-stage FET, τ_s is the shaping time, A_f is the 1/f noise factor of the first-stage FET, q is elementary charge, and I_{leak} is the detector leakage current.

If C_t is the total input capacitance, C_D is the detector capacitance, C_G is the gate capacitance of the first-stage preamplifier FET, and C_p is the parasitic capacitance, then $C_t = C_D + C_G + C_p$. The first term in Eq. (1) represents parallel white noise, the second term represents 1/f series noise, and the third term represents series white noise. An effective way to suppress white parallel noise and 1/f series noise is to lower the total input capacitance C_t.

In this study, for the Φ97 μm micro–readout electrode, a micro–preamplifier fabricated with CMOS technology was installed near the detector and connected by wire bonding to reduce parasitic capacitance. Furthermore, the leakage current I_{leak}, which increases the series white noise, was suppressed by using diamond.

In the case of using diamond single crystals to achieve the same high detection efficiency, sensitive area of 100 mm^2, and energy resolution as those of silicon drift detectors, an energy-spectrometer-grade CVD single-crystal diamond with a sensitive area of 8 × 8 mm^2 has already been reported.[24] Moreover, high-quality substrate crystals of 10 × 10 mm^2 or larger that can be used for crystal growth already exist.[25] On the other hand, the μτ product of diamond is only of 10^{-3} cm^2/V order,[26] even in the highest quality CVD single crystal, which is only 1/1000 of that of silicon (electrons: >1 cm^2/V; holes: ~1 cm^2/V).[27] The charge capture level in diamond is so deep that it is impossible, at this stage, to collect charge by moving the electrons and holes generated by X-rays a few mm laterally as in a silicon drift detector.

As a countermeasure, a multielectrode readout method using multiple microelectrodes, which has been attempted using compound semiconductors with charge carrier transport properties comparable to those of diamond, may be an effective solution. In this method, most of the detector thickness is used as the sensitive area, the readout electrodes are miniaturized, the semiconductor circuit is directly connected to the detector to reduce parasitic capacitance, and the sensitive area is increased by using multiple channels. In fact, there are reports[28] of devices, such as silicon vertex detectors for particle experiments, that contain eight channels of preamplifiers, linear amplifiers, and so forth, fabricated on a silicon chip of about 5 × 5 mm^2 using microfabrication technology.

As the first step toward developing such a detector, we fabricated a prototype diamond X-ray detector consisting of only one channel with a micro–readout electrode of about Φ100 μm on CVD single-crystal diamond, with a micro-CMOS preamplifier placed near the detector and directly connected to it by bonding.

2.2 Fabrication of diamond radiation detector connected to CMOS charge-sensitive preamplifier

Electronics-grade single-crystal CVD diamond from Element Six was used as the diamond. The size of the sample was 3 mm × 3 mm × 300 μm. The surface of the sample was chemically cleaned and oxygen-terminated with hot mixed acid, dichromic acid, and hot aqua regia to ensure high insulation. Then, an Al electrode with a thickness of 100 nm and Φ3 mm was deposited on the incident side by thermal evaporation, and a Ti/Au electrode with a thickness of 100 nm and Φ97 μm was deposited on the readout side by photolithography. The *I–V* characteristics of the sample were then measured at room temperature using a B1505A semiconductor parameter analyzer and a high-vacuum prober. When a voltage of −120 V was applied, the leakage current was confirmed to be about 1 pA (1 × 10^5 pA/m^2) at a room temperature of about 25 °C. The readout electrode and a charge-sensitive preamplifier using CMOS technology manufactured by HORIBA Ltd. with a footprint of about 0.5 × 0.5 mm^2 were then connected to a gold wire using ultrasonic bonding, and these were installed in a detector

mount. The preamplifier was installed on the surface of the readout electrode side of the CVD diamond. Figure 1(a) shows a cross-sectional view of the detector and Fig. 1(b) shows the exterior of the detector. The feedback capacitance of the CMOS preamplifier is very small (13 fF) and was designed to amplify the minute signals generated by soft X-rays. The detector was installed in an aluminum housing to shield it from external electromagnetic noise.

Figure 2 shows a diagram of the circuit used for radiation measurement. The detector shown in Fig. 1(b) was connected to a preamplifier board that supplies power to the CMOS preamplifier and applies the detector bias. An ORTEC 672 shaping amplifier was used. A shaping amplifier gain of 0.67 × 200–1000 and a shaping time of 0.5 μs (the value providing the highest energy resolution) were selected. A WE7562 multichannel analyzer (MCA) (Yokogawa Analytical Systems Inc.) and an ORTEC428 high-voltage power supply were used. A bias voltage of 0 to −300 V was applied to the incident surface electrode side. A LeCroy Wave Surfer 10 digital oscilloscope with an analog bandwidth of 1 GHz was used to measure the output signals of the preamplifier and shaping amplifier. An ^{241}Am γ-ray source of 2.6 × 10^6 Bq and an ^{55}Fe X-ray

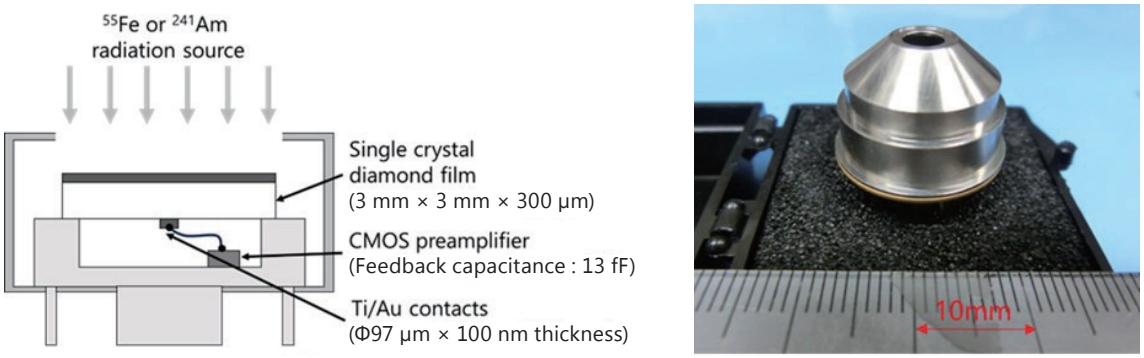

Fig. 1. (Color online) (a) Cross-sectional structure of the detector and (b) appearance of the detector.

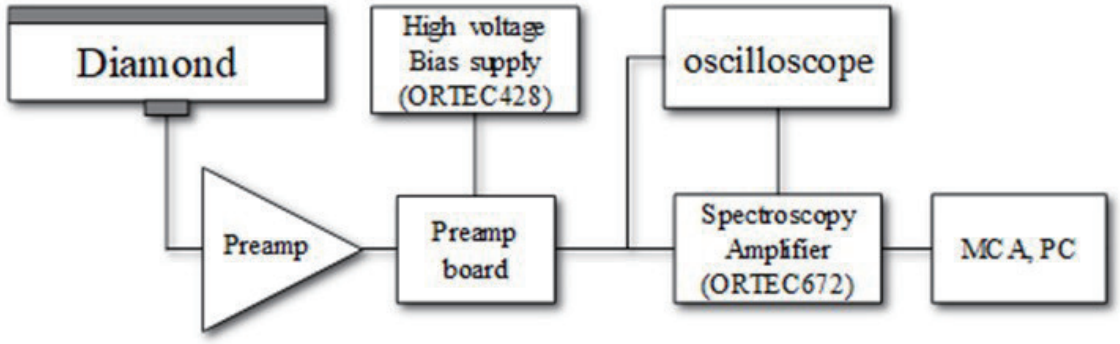

Fig. 2. Radiation measurement circuit diagram. The diamond thin film, preamplifier, and preamplifier board were placed in an Al housing.

source of 0.4×10^6 Bq were used as radiation sources. The sources were placed 2 cm above the plane of the incident electrode, and γ-ray and X-ray measurements were performed in air at room temperature. The counting rates were ~200 cps with the ^{55}Fe source and ~400 cps with the ^{241}Am source, with almost no pile-up.

3. Experimental Results and Discussion

The preamplifier output signal for 5.9 keV X-rays was measured at room temperature using a digital oscilloscope. As the applied voltage was increased, the output voltage increased proportionally, and the output saturated at −300 V. Figure 3(a) shows an example of the output signal of a CMOS preamplifier for 5.9 keV X-rays measured at an applied voltage of −300 V. The maximum wave height of the output signal was about 2 mV and the noise level was 0.5 mmV. An enlarged view of the rising edge of the output signal is shown in the graph in Fig. 3(a). The maximum rise time from 10 to 90% of the output was 20 ns. The steadily rising baseline is due to the ramp wave generated by the charge and discharge of the charge to and from the CMOS preamplifier. Figure 3(b) shows an example of output signal measurement from the main amplifier. The main amplifier has a shaping time of 0.5 μs, a course gain of 1000, and a fine gain of 0.67 as constants. The output wave height was about 1 V. This signal was input to an MCA to measure the energy spectrum.

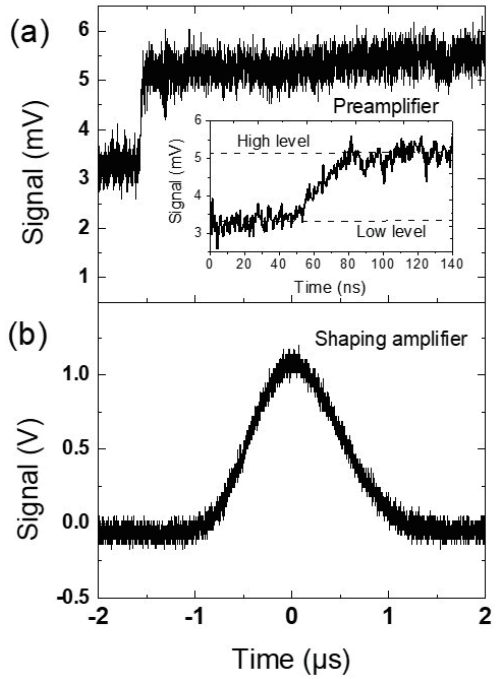

Fig. 3. (a) Example of preamplifier output signal measurement of a diamond soft X-ray detector for 5.9 keV X-rays. The inset shows a magnification of the rising edge of the signal. (b) Example of measurement of the output signal of the shaping amplifier for (a).

Figure 4 shows an example of response function measurement for photons emitted from ^{241}Am. The highest charge collection efficiency and energy resolution were obtained at an applied voltage of −300 V. In this spectrum, the peaks of $L_{\alpha 1}$ at 13.97 keV, $L_{\beta 1}$ at 17.73 keV, $L_{\chi 1}$ at 20.81 and 26.20 keV, and LX at 59.53 keV emitted from ^{241}Am were clearly observed. The highest FWHM of the detector for 59.5 keV calculated using fitting was about 3.8 ± 0.1 keV. The shoulder around 20 keV in the spectrum coincides with the Compton edge at 59.5 keV. In addition, many counts were observed on the low-channel side of each energy peak. Since the background when the source is removed is only a few counts in each channel, the obtained signals originate from radiation.

This phenomenon is caused by the fact that the readout electrode is smaller than the incident surface electrode; thus, the electric field intensity is high only near the readout electrode, and charge carriers generated in other areas are not sufficiently collected. Figure 5 shows the results of a 2D electric field intensity simulation in the thickness direction inside the diamond using the fabricated detector structure. The finite element method using the open-source multiphysics coupled analysis solver Elmer[29] as software was employed for the simulation. Diamond with a size of 3 mm × 3 mm × 300 μm had on both sides of the surface with a potential of −300 V at the Φ3 mm electrode and a potential of 0 V at the Φ100 μm electrode, and the relative permittivity of the diamond was set to 5.7. Simultaneously, the capacitance of the detector was calculated to be

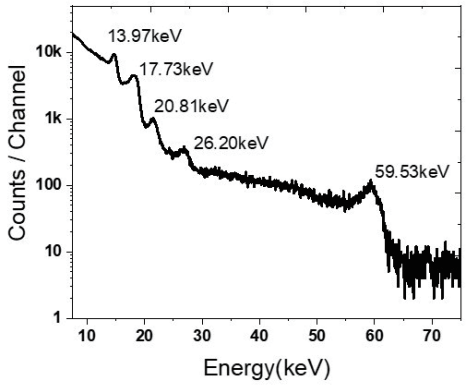

Fig. 4. Example of response function measurement for photons emitted from ^{241}Am. The applied voltage was −300 V.

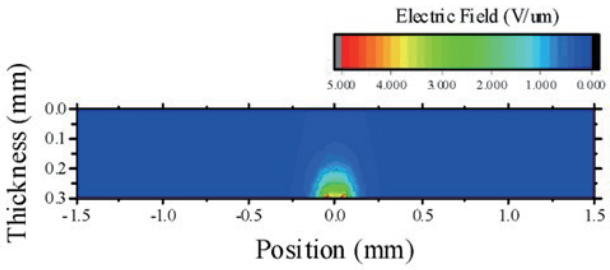

Fig. 5. (Color online) Simulation results of electric field intensity distribution in 300-μm-thick diamond.

120 fF. This value was confirmed to be almost equal to the allowable detector capacitance of the CMOS preamplifier. Values higher than this would result in the degradation of the energy resolution.

In regions other than the collection electrode, the electric field strength is less than 1 V/μm. Because the μτ product is about 10^{-4} cm^2/V, complete charge collection can be expected for charge carriers traveling near the central axis on the readout electrode, but charge collection is expected to be incomplete in other areas. In addition, since the upper output voltage limit of the CMOS charge-sensitive preamplifier used is almost the same as the output of a γ-ray of 59.5 keV, the energy resolution may be degraded if photons are injected at a time earlier than the time constant for recharging the capacitor.

Figure 6 shows an example of detector response function measurement for 5.9 keV X-rays emitted from an ^{55}Fe source. Mn Kα (5.9 keV) and Mn Kβ (6.5 keV) are emitted from the ^{55}Fe source with the probabilities of 24.5 and 3.3%, respectively.[30] Figure 6(a) shows the peak area produced by the 5.9 keV X-rays measured at an applied voltage of −300 V. The energy resolution calculated by Gaussian fitting was about ΔE = (950 ± 20) eV (FWHM). The peak channel value was slightly lower than the expected value obtained from the linearity of ^{241}Am described below. It was not possible to split Mn Kα (5.9 keV) and Mn Kβ (6.5 keV). Next, the same measurement was performed with the applied voltage lowered from −300 to −230 V. The results are shown in Fig. 6(b). In this measurement, the channel width of the MCA was doubled because of the improved energy resolution. Compared with the measurement at −300 V, the switching frequency of the ramp wave was smaller, probably owing to the reduced leakage current. The energy resolution at 5.9 keV was ΔE = (484 ± 10) eV (FWHM), and a broad peak due to Mn Kβ at 6.5 keV was also observed. The measured peak channel count ratio between 5.9 and 6.5 keV was about 10.

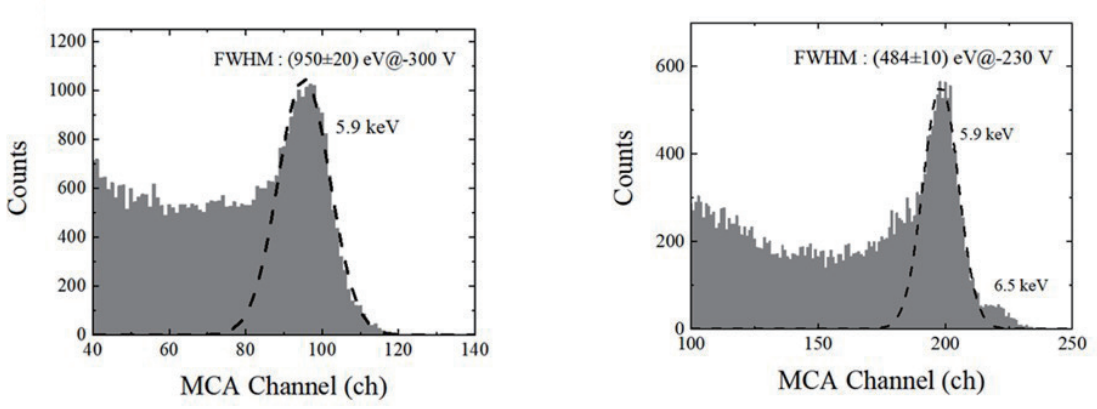

(a) (b)

Fig. 6. Example of detector wave height distribution for 5.9 keV X-rays emitted from an ^{55}Fe source. (a) Applied voltage of −300 V and (b) applied voltage of −230 V with the MCA changed to double the channel width compared with that in (a).

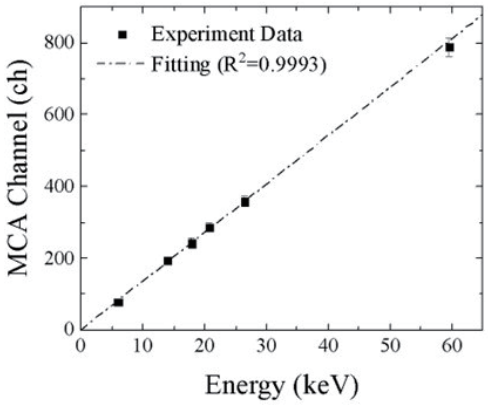

Fig. 7. Linearity of the detector energy response between 5.9 and 59.5 keV. Each plot was obtained from the peak channel of the response function for the energy of radiation emitted from the ^{55}Fe and ^{241}Am sources. Error bars are the FWHM of each peak. The dash-dotted line was obtained by linear fitting of the plots.

5.9 and 6.5 keV are emitted from the ^{55}Fe source with the probabilities of 24.5 and 3.3%, respectively, and the peak channel count ratio of the calculated value was 7.4 if the emission probability is correct. Considering the overlap of the two peaks, the measured and calculated values are close. Although the counts on the low-channel side decreased and the peak became sharper, a broad peak, which was not seen at −300 V, was also observed. However, the energy resolution degraded with time, and eventually, the wave height distribution became similar to that at −300 V.

This phenomenon may be the result of a temporary improvement in the energy resolution owing to two factors: an improvement in charge collection as a result of the filling of charge capture levels (the priming effect), and a decrease in the leakage current because of a reduction in the field strength. The energy resolution may be further improved by suppressing the leakage current using a guard ring.

Figure 7 shows the energy linearity of the measured peak channel values plotted against the radiation energy. The energy resolution of each peak was adopted as the error. The peak channel was found to be highly linear with respect to the radiation energy. The FWHM of the detector increased with decreasing radiation energy. This result indicates that the diamond detector can measure photon energy with sufficient linearity.

4. Conclusions

The response of a diamond radiation detector to photons with energy from 5.9 to 59.5 keV was evaluated toward its application as a soft X-ray energy spectrometer. A diamond soft X-ray detector was fabricated by combining a detector-grade single-crystal diamond sample with a micro-CMOS charge-sensitive preamplifier with a feedback capacitance of 13 fF designed for soft X-ray measurements. The energy resolution of the fabricated detector was 3.8±0.1 keV for

59.5 keV γ-rays. The broad counts at low energies were due to incomplete charge collection in the low-field region. The response to ^{55}Fe X-rays was also evaluated. The energy resolution for 5.9 keV X-rays was $\Delta E = (484 \pm 10)$ eV (FWHM), and a broad peak at 6.5 keV was also observed. The reason for the improved energy resolution may be a combination of two effects: priming and reduced leakage current. The energy linearity obtained from the peak channel values corresponding to energies from 5.9 to 59.5 keV was sufficiently linear with a decision count of $R^2 = 0.9993$. These results indicate that the single-crystal diamond detector has potential for practical use as a soft X-ray detector that can be operated at room temperature. In the future, we aim to achieve sufficient charge collection efficiency over the entire crystal by increasing the number of channels in the readout electrode and to further develop the detector so that it can be used in practical applications.

References

1 C. Bauer, I. Baumann, C. Colledani, J. Conway, P. Delpierre, F. Djama, W. Dulinski, A. Fallou, K. K. Gan, R. S. Gilmore, E. Grigoriev, G. Hallewell, S. Han, T. Hessing, K. Honschied, J. Hrubec, D. Husson, H. Kagan, D. Kania, R. Kass, W. Kinnison, K. T. Knopfle, M. Krammer, T. J. Llewellyn, P. F. Manfredi, L. S. Pan, H. Pernegger, M. Pernicka, R. Plano, V. Re, S. Roe, A. Rudge, M. Schaeffer, S. Schnetzer, S. Somalwar, V. Speziali, R. Stone, R. J. Tapper, R. Tesarek, W. Trischuk, R. Turchetta, G. B. Thomson, R. Wagner, P. Weilhammer, C. White, H. Ziock, and M. Zoeller: Nucl. Instrum. Methods Phys. Res., Sect. A **367** (1995) 207. https://doi.org/10.1016/0168-9002(95)00545-5

2 W. Adam, W. de Boer, E. Borchi, M. Bruzzi, C. Colledani, P. D'Angelo, V. Dabrowski, W. Dulinski, B. van Eijk, V. Eremin, F. Fizzotti, H. Frais-Kolbl, C. Furetta, K. K. Gan, A. Gorisek, E. Griesmayer, E. Grigoriev, F. Hartjes, J. Hrubec, F. Huegging, H. Kagan, J. Kaplon, R. Kass, K. T. Knopfle, M. Krammer, W. Lange, A. Logiudice, C. Manfredotti, M. Mathes, D. Menichelli, M. Mishina, L. Moroni, J. Noomen, A. Oh, H. Pernegger, M. Pernicka, R. Potenza, J. L. Riester, A. Rudge, S. Sala, S. Schnetzer, S. Sciortino, R. Stone, C. Sutera, W. Trischuk, J. J. Velthuis, B. Vincenzo, P. Weilhammer, J. Weingarten, N. Wermes, and W. Zeuner: Nucl. Instrum. Methods Phys. Res., Sect. A **565** (2006) 278. https://doi.org/10.1016/j.nima.2006.05.127

3 W. D. Boer, J. Bol, A. Furgeri, S. Muller, C. Sander, E. Berdermann, M. Pomorski, and M. Huhtinen: Phys. Status Solidi A **204** (2007) 3004. https://doi.org/10.1002/pssa.200776327

4 V. Grilj, N. Skukan, M. Jakšić, W. Kada, and T. Kamiya: Nucl. Instrum. Methods Phys. Res., Sect. B **306** (2013) 191. https://doi.org/10.1016/j.nimb.2012.12.034

5 M. Angelone, N. Fonnesu, M. Pillon, G. Prestopino, F. Sarto, E. Milani, M. Marinelli, C. Verona, and G. Verona-Rinati: IEEE Trans. Nucl. Sci. **59** (2012) 2416. https://doi.org/10.1109/TNS.2012.2210735

6 M. Tsubota, J. H. Kaneko, D. Miyazaki, T. Shimaoka, K. Ueno, T. Tadokoro, A. Chayahara, H. Watanabe, Y. Kato, S. Shikata, and H. Kuwabara: Nucl. Instrum. Methods Phys. Res., Sect. A **789** (2015) 50. http://doi.org/10.1016/j.nima.2015.04.002

7 R. Pilotti, M. Angelone, M. Marinelli, E. Milani, G. Verona-Rinati, C. Verona, G. Prestopino, R. M. Montereali, M. A. Vincenti, E. M. Schooneveld, A. Scherillo, and A. Pietropaolo: Euro. Phys. Lett. **116** (2016) 42001. https://doi.org/10.22323/1.240.0180

8 A. Kumar, A. Kumar, A. Topkar, and D. Das: Nucl. Instrum. Methods Phys. Res., Sect. A **858** (2017) 12. https://doi.org/10.1016/j.nima.2017.03.033

9 J. Isberg, J. Hammersberg, E. Johansson, T. Wikström, D. J. Twitchen, A. J. Whitehead, S. E. Coe, and G. A. Scarsbrook: Science **297** (2002) 1670. https://doi.org/10.1126/science.1073869

10 M. J. Guerrero, D. Tromson, M. Rebisz, C. Mer, B. Bazin, and P. Bergonzo: Diam. Relat. Mater. **13** (2004) 2046. https://doi.org/10.1016/j.diamond.2004.07.026

11 M. Pomorski, E. Berdermann, M. Ciobanu, A. Martemyianov, P. Moritz, M. Rebisz, and B. Marczewska: Phys. Status Solidi A **202** (2005) 2199. https://doi.org/10.1002/pssa.200561929

12 J. H. Kaneko, T. Tanaka, T. Imai, Y. Tanimura, M. Katagiri, T. Nishitani, H. Takeuchi, T. Sawamura, and T. Iida: Nucl. Instrum. Methods Phys. Res., Sect. A **505** (2003) 187. https://doi.org/10.1016/S0168-9002(03)01048-9

13 G. J. Schmid, J. A. Koch, R. A. Lerche, and M. J. Moran: Nucl. Instrum. Methods Phys. Res., Sect. A **527** (2004) 554. https://doi.org/10.1016/j.nima.2004.03.199

14 C. Cazzaniga, M. Nocente, M. Rebai, M. Tardocchi, P. Calvani, G. Croci, L. Giacomelli, M. Girolami, E. Griesmayer, G. Grosso, M. Pillon, D. M. Trucchi, and G. Gorini: Rev. Sci. Instrum. **85** (2014) 11E101. https://doi.org/10.1063/1.4885356
15 M. Rębisz, B. Voss, A. Heinz, E. Usenko, and M. Pomorski: Diamond Relat. Mater. **16** (2007) 1070. https://doi.org/10.1016/j.diamond.2006.12.053
16 Y. Sato and H. Murakami: Jpn. J. Appl. Phys. **54** (2015) 096401. https://doi.org/10.7567/JJAP.54.096401
17 S. F. Kozlov, R. Stuck, M. Hage-Ali, and P. Siffert: IEEE Trans. Nucl. Sci. **NS-22** (1975) 160. https://doi.org/10.1109/TNS.1975.4327634
18 P. Lechner, C.Fiorini, R. Hartmann, J. Kemmer, N. Krause, P. Leutenegger, A. Longoni, H. Soltau, D. Stotter, R. Stotter, L. Struder, and U. Weber: Nucl. Instrum. Methods Phys. Res., Sect. A **458** (2001) 281. https://doi.org/10.1016/S0168-9002(00)00872-X
19 M. Kurakado, E. C. Kirk, S. Shiki, H. Sato, K. Mishima, C. Otani, and K. Taniguchi: Nucl. Instrum. Methods Phys. Res., Sect. A **621** (2010) 431. https://doi.org/10.1109/TNS.1975.4327634
20 G. Conte, M. Girolami, S. Salvatori, and V. Ralchenko: Appl. Phys. Lett. **91** (2007) 183515. https://doi.org/10.1063/1.2805221
21 Z. Minglong, X. Yiben, W. Linjun, and S. Hujiang: Solid State Commun. **130** (2004) 425. https://doi.org/10.1016/j.ssc.2004.01.013
22 J. E. Lees, D. J. Bassford, E. J. Bunce, M. R. Sims, and A. B. Horsfall: Nucl. Instrum. Methods Phys. Res., Sect. A **604** (2009) 174. https://doi.org/10.1016/j.nima.2009.01.050
23 G. Bertuccio and A. Pullia: Rev. Sci. Instrum. **64** (1993) 3294. https://doi.org/10.1063/1.1144293
24 S. Hirano, J. H. Kaneko, T. Hanada, S. Ito, T. Shimaoka, H. Shimmyo, M. Tsubota, A. Chayahara, Y. Mokuno, and H. Umezawa: Phys. Status Solidi A **215** (2018) 1800333. https://doi.org/10.1002/pssa.201800333
25 H. Sumiya and K. Tamasaku: Jpn. J. Appl. Phys. **51** (2012) 090102. https://doi.org/10.1143/JJAP.51.090102
26 J. Isberg, J. Hammersberg, H. Bernhoff, D.J. Twitchen, and A.J. Whitehead: Diam. Relat. Mater. **13** (2004) 872. https://doi.org/10.1016/j.diamond.2003.11.065
27 A. Owens and A. Peacock: Nucl. Instrum. Methods Phys. Res., Sect. A **531** (2004) 18. https://doi.org/10.1016/j.nima.2004.05.071
28 S. Kishimoto, S. Shimazaki, M. Ikeno, M. Saito, T. Taniguchi, and M. Tanaka: 2011 IEEE Nucl. Sci. Symp. Conf. Rec. (2011) 1674. https://doi.org/10.1109/NSSMIC.2011.6154659
29 Elmer: https://www.csc.fi/web/elmer (accessed October 2023).
30 U. Schötzig: Appl. Radiat. Isot. **53** (2000) 469. https://doi.org/10.1016/s0969-8043(00)00166-4